available at www.sciencedirect.com

ScienceDirect

journal homepage: www.elsevier.com/locate/jmbbm

Research paper

Impact of thermomechanical texture on the superelastic response of Nitinol implants

M.M. Barney[a,1], D. Xu[b], S.W. Robertson[a], V. Schroeder[c], R.O. Ritchie[b], A.R. Pelton[a], A. Mehta[d,*]

[a] NDC, 47533 Westinghouse Dr., Fremont, CA 94539, United States
[b] Materials Sciences Division, Lawrence Berkeley National Laboratory, and Department of Materials Science and Engineering, University of California, Berkeley, CA 94720, United States
[c] Cordis Corporation, 6500 Paseo Padre Parkway, Fremont, CA 94555-3658, United States
[d] Stanford Synchrotron Radiation Lightsource, SLAC National Accelerator Laboratory, Menlo Park, CA 94025, United States

ABSTRACT

The phenomenon of superelasticity in near-equiatomic NiTi, which originates from a first-order martensitic phase transition, is exploited in an increasing number of biomedical devices, most importantly endovascular stents. These stents are often manufactured from microtubing, which is shown to be highly textured crystallographically. Synchrotron X-ray microdiffraction provided microstructural, phase, and strain analysis from Nitinol tube sections that were deformed in situ along longitudinal, circumferential, and transverse orientations. We show that the large variation in the superelastic response of NiTi in these three tube directions is strongly influenced by the path that the martensitic transformation follows through the microstructure. Specifically, in severely worked NiTi, bands of ⟨100⟩ grains occur whose orientation deviates markedly from the surrounding matrix; these bands have an unusually large impact on the initiation and the propagation of martensite, and hence on the mechanical response. Understanding the impact of these local microstructural effects on global mechanical response, as shown here, leads to a much fuller understanding of the causes of deviation of the mechanical response from predictions and unforeseen fracture in NiTi biomedical devices.

Published by Elsevier Ltd

1. Introduction

Deployment of self-expanding stents, manufactured from near-equiatomic NiTi (Nitinol) is an effective, lower risk therapy alternative to surgery and represents a major therapy in the fight against cardiovascular disease (Schillinger et al., 2006). Due to the first-order phase transition from cubic austenite (B2) to monoclinic martensite (B19') phase, Nitinol can undergo several times larger reversible deformation than conventional biomaterials such as stainless steel or

titanium. This feature makes Nitinol optimally compliant to withstand large crimp and deployment strains (up to 10%) as well as cyclic deformations experienced by the peripheral vessels, while maintaining vessel patency. Indeed, such superelasticity in Nitinol has been exploited in many other biomedical applications, from endodontic files to spinal prostheses (Duerig et al., 1996).

Nitinol biomedical devices are manufactured from wires, thin rods, sheet, strip or thin-walled tubes, all of which are formed by a series of hot and cold working operations from cast ingots to final shape. The multistage thermomechanical processes impart deformations that significantly affect the microstructure (grain size, defect density, and crystallographic orientation). For example, there is a million-fold reduction in the cross sectional area in fabricating a 0.5 mm diameter wire from the original (500 mm diameter) as-cast ingot. As such, the grain refinement and crystallographic texture formation resulting from these manufacturing processes can be considerable.

Fig. 1 shows two versions of a generic stent pattern (http://nitinoluniversity.com/open-stent-design/) laser cut from thin-walled Nitinol tubes. The as-cut pattern (a) is from a 2 mm diameter tube (the so-called "closed configuration"), whereas the pattern in (b) is from an 8 mm diameter tube ("open configuration").[2] After mechanical expansion of both stents to 10 mm diameter and "shape setting" (stress relief at ~500 °C), the stent that was laser machined in the closed configuration (c) is macroscopically identical to that of open configuration stent (d). Note, however, that the orientation of the tube axis, and hence the drawing direction (indicated by the arrow) relative to the major axis of the struts in the open and the closed configuration of stents, are significantly different. As demonstrated by Pelton et al. (2008), the radial pressure exerted by a Nitinol stent is proportional to the mechanical properties of the individual "V" sections of the final stent geometry. Though still poorly understood, the influence of microstructural orientation on the superelastic response of NiTi is known to be significant (Robertson et al., 2006). Consequently, differences in crystallographic texture for macroscopically identical stents may result in stents experiencing markedly different cumulative radial forces and fatigue properties.

Cardiac cycles and musculoskeletal motions subject biomedical devices to millions of complex deformations. For example, a stent deployed in the superficial femoral artery (SFA) undergoes severe multiaxial displacements from pulsatile motion (ca. 4×10^7 cycles annually) plus up to 60% rotation and up to 20% contraction (at a rate of ca. 1×10^6 cycles annually) as the leg is bent during a walking cycle (Cheng et al., 2006, 2010). To design a device to withstand these frequent and severe deformations, finite element analytical (FEA) models of complex structures such as endovascular stents are generated by creating a fine elemental mesh of the geometry (Rebelo and Perry, 2000). The models attempt to

incorporate the highly nonlinear mechanical response of NiTi from global monotonic stress–strain relationships. But as the microstructural and textural effects alluded to above are still poorly understood, they are ignored in current commercially available computational design models; this leads to predictions that are only qualitative and deviate significantly from the actual response at large deformation, as demonstrated previously (Mehta et al., 2007). Occasionally, therefore, an implant unexpectedly fractures *in vivo*, resulting in loss of vessel patency, and requires a major invasive surgery (Pelton et al., 2008).

X-ray microdiffraction (μXRD) from a synchrotron radiation source was the primary tool used to characterize the microstructural features, including grain size and grain orientation. This technique is the only method with sufficient spatial resolution (<10 μm) to allow detailed analysis of a 'bulk' specimen on the order of a stent strut. Furthermore, this technique provides the highest resolution strain gauge that can distinguish among different modes of strain accommodation, *i.e.*, elastic, plastic, or phase transformational strain.

Consequently, the goal of the investigation reported here is to develop a deeper understanding of the role of microstructure and texture on the martensite phase transformation and superelastic response.

2.   Material and method

Medical-grade $Ni_{50.8}Ti_{49.2}$ tubing (5.5 mm OD with 0.3 mm wall thickness) was laser machined along the longitudinal axis. These tube sections were then shaped into flattened "sheets" by a two-step process at 500 °C. This flattening process induced approximately 10% strain into the material, comparable to the expansion strains used during forming endovascular Nitinol stents from laser-machined tubes (Pelton et al., 2000), but insignificant in comparison to the strain introduced on formation of the tube from the ingot. Micro-dogbone-shaped tensile specimens were then laser machined from these flattened sheets at three different orientations to the Nitinol tube drawing axis: 0°, (longitudinal), 45° (transverse), and 90° (circumferential); see Fig. 2 inset for a photograph of a dogbone. The dogbone specimens were given an additional heat treatment of 700 °C for five minutes to obtain a nominal austenite grain size of about 10–20 μm. The larger grain size was necessary to permit the 1 μm X-ray spot size to resolve the grain-by-grain transformation. These thermal treatments resulted in an austenite finish temperature of 15 °C, as measured by the bend-free recovery method in accordance with ASTM F 2082 (2006). After electropolishing, these dogbones had a gauge section of $800 \times 200 \times 200$ μm.

Global force–displacement curves were obtained at room temperature from dogbone specimens machined in the three different orientations, using a 2.3 kg_f maximum force capacity displacement-controlled rig. The measurements were performed at room temperature on the same *in situ* rig used for the microdiffraction measurements. The rig grips had 2 mm diameter alignment pins to hook the corresponding machined alignment holes in the flared grip section of the dogbone. The rig displacement was gradually

---

[2] The terms "open" and "closed" configuration refer to the manner in which the stents are manufactured and should not be confused with "open" and "closed" cell geometry verbiage used in stent design.
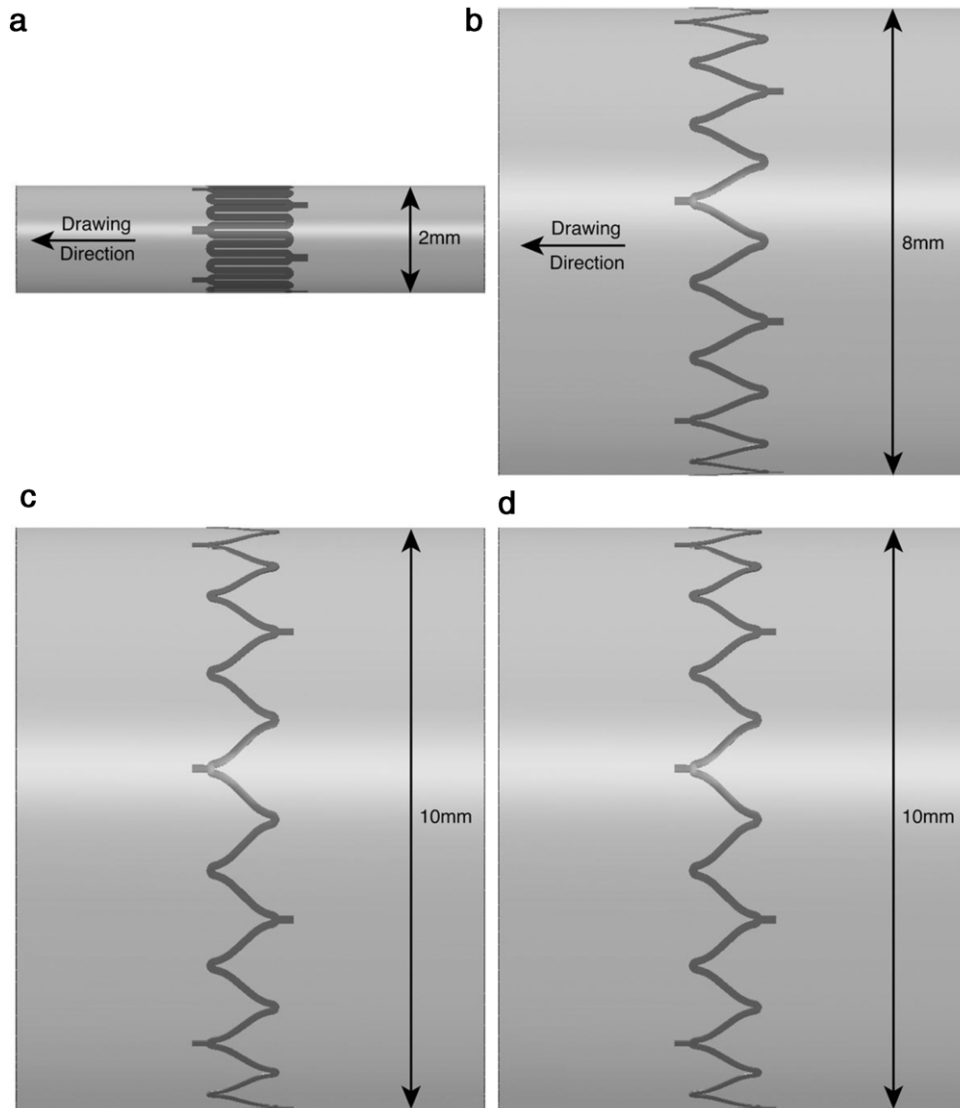
Fig. 1 – Illustration of the effects of starting tube diameter to produce a 10 mm diameter Nitinol stent. Fig. 1(a) shows the as-cut layout of a row of a generic stent from a 2 mm tube ("closed configuration"). Note that the struts align with the tube drawing direction. Fig. 1(b) shows the same stent laid out on an 8 mm tube ("open configuration"). In this case, the struts are aligned at an angle to the tube drawing direction. Fig. 1(c) and (d) show the stents when expanded to their final 10 mm dimension.

increased until the load cell just began to register a small tensile load; at that instant the flared end of the dogbones were firmly bolted to the grips. Positions of small Pt markers deposited via focused ion beam at the two grip ends were monitored to confirm that the dogbones did not slip in the grips on loading. However, other elastic deformations outside of the sample gauge contributed to the overall extension. Since the samples were of identical dimension, deformation is reported in units of displacement of the moving grip rather than strain. This approach is sufficient for this study to provide a relative comparison of the global strain response. The samples were deformed at the displacement rate of 0.1 μm/s, which is slow enough to provide isothermal conditions. The direction of loading was reversed after a slope of the stress plateau just began to increase. The measurement was completed when the force returned to zero. Measurements repeated for several specimens of the same orientation demonstrated similar force–displacement curves. See Fig. 2 for an image of the straining rig in place at the Advanced Light Source beamline; the inset image is a close-up of the Nitinol dogbone specimen mounted onto the rig.

A 1 μm diameter X-ray beam was used to scan the entire gauge section (800 × 200 μm) of the samples using a 6–10 μm step size, yielding between 4800–6400 diffraction patterns per specimen per strain condition. White beam Laue diffraction patterns from the entire gauge section were obtained at each level of deformation. These Laue diffraction patterns yielded the full three-dimensional deviatoric strain tensor as well as the local orientation of the austenite crystal lattice (grain orientation) (Tamura et al., 2002). Unlike measurement of global strain (macro-strain), measurement of elastic
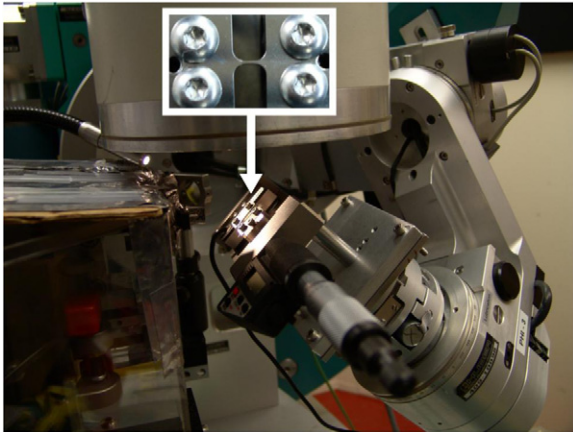
Fig. 2 – Photograph of the straining rig in place at the ALS beamline 7.3.3. Inset is a higher magnification image of the dogbone specimen used in these studies.

Fig. 3 – Global uniaxial tensile stress–strain curves for Nitinol machined in the longitudinal, transverse, and circumferential directions, i.e., respectively, 0°, 45°, and 90° to the drawing direction.

strain (lattice strain) via polychromatic microdiffraction is not dependent on external gauges or references. Strain measurements are shown to be precise and greater than a few parts in 10,000 with this method. Martensite nanocrystalline laths are too small for the micrometer-sized white beam to probe (Robertson et al., 2007); consequently, the absence of a Laue diffraction pattern indicated the presence of martensite. The fraction of the gauge length that transformed was determined by counting the number of martensite pixels in a phase map and dividing it by the total number of pixels in the gauge length. Simultaneous uniaxial force–displacements were also obtained so that direct correlations could be made to chart the dynamic phase transformation events.

3.   Results and discussion

3.1.   Global mechanical anisotropy

Fig. 3 shows the global "superelastic" stress–displacement curve consisting of two linear elastic regions separated by a "stress plateau" for the 0°, 45°, and, 90° specimen orientations. The 0° and 90° samples were nominally identical and match the predictions of martensitic theories of single crystals (Bhattacharya, 2003). However, every characteristic of the 45° specimens, including the stress at the onset, slope, and length of the superelastic "plateau", displayed a significantly different behavior. Furthermore, these 45° characteristics also differ considerably from the theoretical predictions. The oscillations in the stress plateaus observed in these curves are due to the interaction of the advancing stress-induced martensite fronts with the microstructure (Eucken and Duerig, 1989). These features in "global" force–displacement clearly point to differences in the propagation of stress-induced martensite and will be discussed in much greater detail below.

Differences in mechanical response in Nitinol were also observed when the mode of deformation (i.e., tension, compression, bending, and torsion) was varied in superelastic wire (Wick et al., 1995) and tube specimens (McNaney et al.,
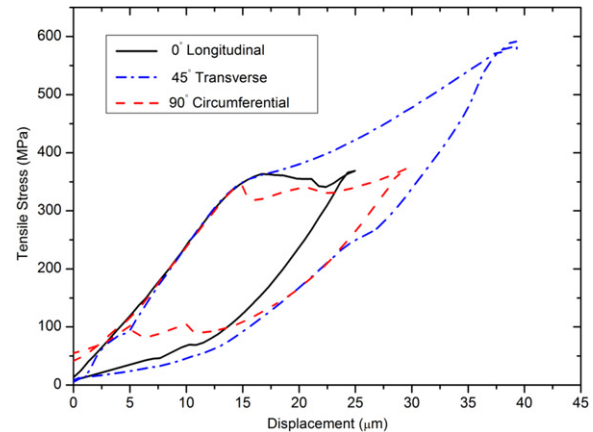
2003). Furthermore, such anisotropies in mechanical and shape memory behavior were observed in Nitinol specimens produced from sheets with different orientations. Specifically, Mulder et al. (1994) while investigating the anisotropy of thermal fatigue properties of cold-rolled and aged $Ni_{50.8}Ti_{49.2}$ sheet observed the greatest difference in transformation temperatures and fatigue properties between specimens machined from the rolling direction (RD) and the transverse direction (TD). Conventional XRD texture analysis of their sheet indicated that there was a tendency for $(010)[001]_M$ martensite texture along the RD whereas the TD contained a combination of $(111)[1\bar{1}\bar{1}]_M$ and $(11\bar{1})[1\bar{1}1]_M$ martensite. Liu et al. (1999) correlated the mechanical properties and microstructures (by transmission electron microscopy) of near-equiatomic NiTi sheet that had 30% cold work followed by 30 min anneals at 300–800 °C. They observed, for example, that the stress plateau length in the RD was approximately twice as long as that in the TD. Crystallographic analysis based on the texture measurements suggests that the rolling direction is more favorable to the shear direction of $\langle 011 \rangle_M$ type II martensite twins, while the transverse direction is more favorable to the shear direction of $(001)_M$ compound twins. Robertson et al. (2006) showed that the crystallographic anisotropies in Nitinol wire and tubing are dramatically different and substantially more severe than in sheet. For example, in drawn products the texture is $\{221\}\langle 12\bar{2}\rangle$, whereas in the rolled product, it is similar to rolled α-iron, namely, $\{111\}\langle 11\bar{2}\rangle$. With these dominant textures, the calculated and experimentally observed transformational strains for the drawn material are at a minimum at 45° to the drawing direction, whereas, 90° is comparable to that at 0°. In contrast, the calculated maximum transformation strain is in the sheet RD and minimum in the TD, in accordance with the experimental results from Mulder et al. (1994), Liu et al. (1999) and Hasan et al. (2008). Surprisingly, Robertson et al. (2006) showed that the crystallographic texture in nanocrystalline and fully annealed wires and tubes were not significantly different; specifically, they analyzed tubing after aging (485 °C) and annealing (850 and 1100 °C), and
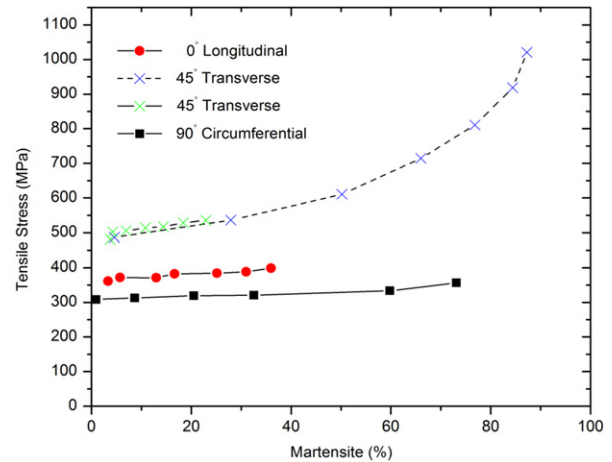
observed that the texture did not change even though the grain size grew by a thousand-fold to 75 μm at the highest annealing temperature. This result strongly implies that the texture is formed primarily during the million-fold reduction during the initial tube fabrication and is less affected by subsequent treatments, such as shape setting or annealing even with dramatic grain growth. As such, it is expected that the findings in the present work with ∼20 μm grain size are generally applicable to any other product formed from tubes, irrespective of the grain size (nanocrystalline to highly crystalline) or shape.

There is growing evidence that the highly textured microstructure of thermomechanically processed NiTi is the cause of the large variation in the stress–strain behavior observed in the three orientations in Fig. 3. This orientation-dependent mechanical behavior, which has not been reported before in Nitinol tubing, suggests that the two macroscopically identical stents shown in Fig. 1 will have a significantly different mechanical response. These data additionally explain why past attempts to estimate the superelastic mechanical response by codifying phenomenological bulk stress–strain curves (Jung et al., 2004; Rebelo and Perry, 2000) have not been very successful. Thus, to understand the global mechanical response of a superelastic material, a microstructural understanding of the relationship among the grain orientation, phase transformation pattern, and local stress distribution is essential.

3.2. Martensitic transformation and global mechanical behavior

The impact of the pattern of martensitic transformation on the global mechanical behavior[3] is most clearly seen in a plot of the externally applied stress *versus* the fraction of the gauge length transformed to martensite. Fig. 4 shows such relationship for 0°, 45°, and 90° specimens obtained from our *in situ* μXRD measurements. Comparison among curves with different orientations mimics the differences seen in Fig. 3 in the features of the superelastic plateau. The 45° specimens differ from the 0° (and the 90°) specimen in three distinct ways: (i) stress at which transformation plateau begins, (ii) the slope of the plateau, and (iii) the percentage of martensite at the end of the macroscopic stress plateau. Since the 0° and 90° orientations have comparable global mechanical response, texture, and strain distribution, for the purposes of this paper, they will henceforth be collectively called 0° specimens. Table 1 summarizes these three distinct differences in the way the gauge length transforms to martensite between the three orientations of specimens.

The 0° specimens begin to transform when the macroscopic tensile stress is nominally 350 MPa, whereas the macroscopic plateau does not appear in the 45° sample

---

[3] Here we define the global behavior as the cumulative stress–strain response of the entire collective of grains that comprise the gauge section. As such the macroscopic tensile stress is equal to the applied load divided by the gauge cross sectional area and the global strain is the change in gauge length divided by the original length.

Fig. 4 – The variation in % martensite transformed as a function of the tensile stress, as measured during the *in situ* deformation of Nitinol dogbone samples, machined in the longitudinal, transverse, and circumferential directions, i.e., respectively, 0°, 45°, and 90° to the drawing direction.

until the macroscopic tensile stress reaches approximately 500 MPa, showing a 40%–60% higher stress required for the onset of stress-induced martensite. Initial progression of transformation in the 0° (or the 90°) specimens requires very little additional stress, resulting in a fairly flat plateau in the stress–strain response. On the other hand, even after the onset of transformation in the 45° specimens, further transformation requires significant additional stress, leading to a plateau with a distinctly upward slope. Finally, contrary to common belief, the end of the plateau region does not coincide with complete transformation to martensite for these specimens. Even for the easily transformable 0° specimen, when the applied stress begins to increase, effectively ending the global stress–strain plateau, as much as 20% of the gauge length has remained untransformed. In a recent paper, Young et al. (2010) also observed a variation in martensitic transformation along the length of a superelastic wire that was macroscopically strained to the end of the stress plateau. In contrast to the present work, however, they observed that over 96% of the austenite transforms to martensite at strains slightly above the stress plateau.[4] For the 45° specimen the transformation plateau is even shorter with as much as 50% of the gauge untransformed before the stress begins to increase steeply again. These differences in tensile behavior between the 0° and 45° specimens are similar to that observed in the RD and TD sheet specimens, as discussed above (Mulder et al., 1994).

---

[4] Young et al. (2010) also measured the elastic moduli with (100), (110), (200) and (211) reflections. Although it is beyond the scope of the present paper, a companion transmission μXRD study measured the elastic moduli from nanocrystalline Nitinol thin films, Pelton et al. (unpublished results), to be 73 GPa (100, 200), 89 GPa (110), 90 GPa (211) and the crystallographic elastic anisotropy of 1.3 respectively. Though the Young and Pelton measurements are in qualitative agreement, there are significant differences in specific details that will be addressed in Pelton et al. publication.

Table 1 – Characteristics of the uniaxial stress/strain behavior of the 0°, 45° and 90° Nitinol specimens.			
	Initial transformation plateau stress (MPa)	Plateau slope (MPa)	Percent martensite at plateau termination (%)	Dominant grain orientation
0° specimen	350	~400[a]	~80	⟨111⟩
45° specimen	500	~2000	~50	⟨100⟩
90° specimen	300	~400[a]	~80	⟨110⟩

[a] The slopes of the plateau for the 0° and 90° specimens are difficult to determine because of large non-monotonic variations.
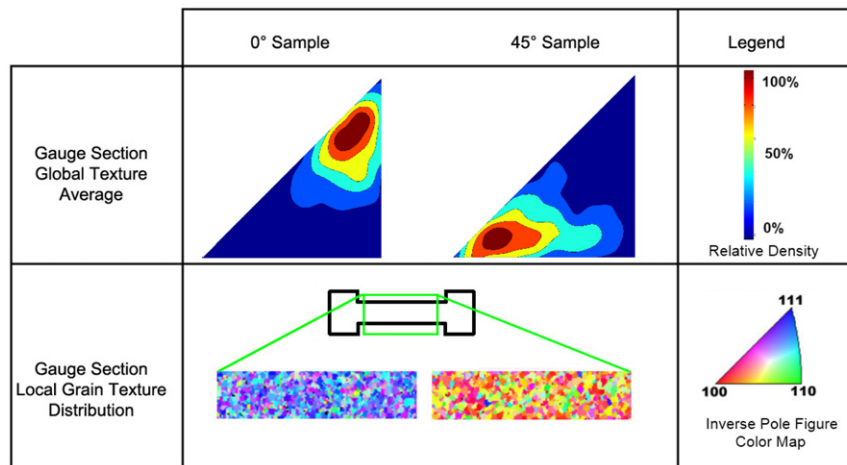
Fig. 5 – The local texture variations versus the global averaged textures. 0° samples have an averaged texture of ⟨111⟩, whereas 45° samples have an averaged texture of ⟨100⟩. The local distributions show the existence grains that are highly misoriented from the global average.

3.3. Local transformation pattern and elastic strain map

As presented above, austenite in the 0° and 45° specimens appears to transform in a markedly different manner, leading to different superelastic responses. In an attempt to understand these differences at the microstructural level, we probed the transformation at the scale of individual grains. Fig. 5 shows a map of the local grain orientation (along the deformation axis) with the global texture shown on an inverse pole figure for the 0° and 45° specimens. Naturally, as these samples were cut from tubes that undergo thermomechanical drawing deformation, they are not only heavily textured but have dramatically different crystallographic texture from each other. The 0° specimens have predominantly ⟨111⟩-type grains, whereas 45° specimens have predominantly ⟨100⟩-type grain orientations along the deformation axis. Notably, there are clusters of grains in both orientations that are significantly misoriented with respect to their neighbors and the average grain orientation (i.e., global texture). This is most easily noticeable for ⟨100⟩-orientated grains, seen to form narrow bands spaced along the length of the specimen.

Fig. 6 shows the austenite elastic strain maps for both orientations with progressively increasing tensile deformations. The blackened pixels, increasing in population going down a column, are regions that have transformed to martensite. The figure shows that the way the austenite transforms to martensite and the way elastic strain distributes along the gauge are significantly different between the 0° and 45° orientations. Nevertheless, there are many

characteristics of the transformation that are common to all orientations. For the three orientations investigated here, the gauge length transformed through multiple nucleation events that appear to occur frequently at grain boundaries (often at high-angle grain boundaries) near ⟨111⟩ and ⟨110⟩ type grains, similar to that shown by Kröger et al. (2006). The growth of martensite from this nucleation point is irregular; the transformation front occasionally "leap-frogs", leaving behind islands of untransformed austenite. The resulting transformed region is almost never contiguous. In many macroscopic measurements, especially on nanocrystalline materials deformed at high strain rates, superelastic transformation appears to form a uniform, Lüders-like band, but even in some optical measurements of larger grain material and at low deformation rate transformation region appears to be far from homogeneous (Brinson et al., 2004). Furthermore, most of the austenite grains in the specimens bear no more than 1.2% elastic strain, even when the average macroscopic strain is several times greater. Young et al. (2010) and Pelton et al. (unpublished results) in their transmission μ-XRD investigations of Nitinol show that the elastic strain in transformed martensite is even less than in austenite; therefore, transformational strain accounts for a large fraction of strain with increasing deformation. The islands of trapped and untransformed material, on the other hand, are the exception to this observation.

The most difficult grains to transform appear to be those with ⟨100⟩ orientation, in agreement with observations of shape memory transformations in single crystals
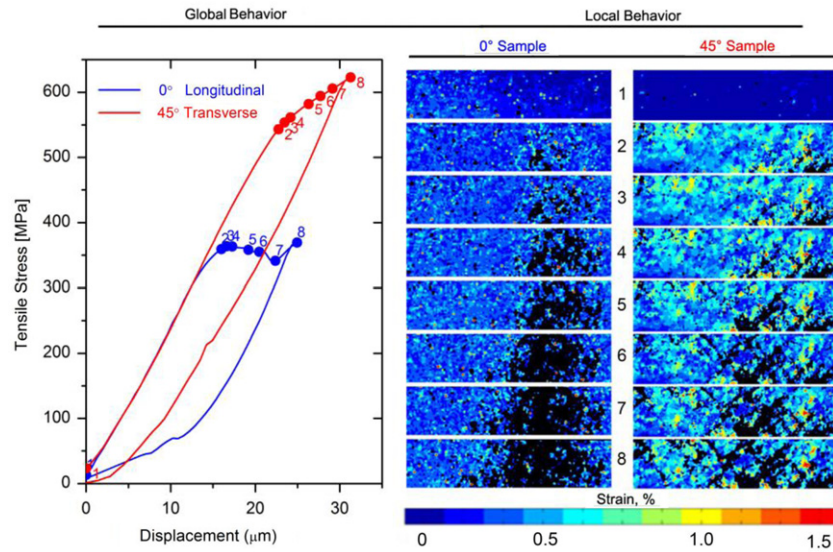
Fig. 6 – The strain evolution of 0° and 45° samples as a function of increasing deformation. Both samples develop region of transformed martensite (black), however the morphology of transformed region is different. 0° samples have flat, nearly uniform region, whereas 45° samples develops highly heterogeneous diagonal bands that cuts across the samples. Furthermore, both sets of samples feature regions of austenite that are highly strained, beyond the typical 1.2% threshold for martensite transformation.

(Miyazaki et al., 1984). In contrast, the transformational stress for ⟨111⟩ and ⟨110⟩ orientations are quite similar and significantly lower than the ⟨100⟩ orientation. These observations can be partially explained by considering the Taylor factor for the shape strain among the various grain orientation variants under the influence of applied stress (Ono and Sato, 1988; Ono et al., 1989; Bhattacharya, 2003; Robertson et al., 2006). Furthermore, our observations indicate that when a grain transforms, it frequently reduces the elastic strain, and hence the stress, on adjacent grains. A similar stress reduction is also observed in macroscopic measurements (Shaw and Kyriakides, 1997). Often this local stress redistribution results in a redirection of the transformation front that, in some cases, encircles a region of untransformed austenite. Grains entrapped in an island in this manner have no dominant orientation and often transform subsequently. Robertson et al. (2007) also observed a similar redirection of the transformation front around a ⟨100⟩ grain as part of an *in situ* μXRD investigation of an advancing crack in fatigued Nitinol. However, trapped islands of predominantly ⟨100⟩ type grains bear progressively larger strains and often require significantly greater applied stress for transformation. The inability of the ⟨100⟩ type grains to transform results in the plateau ending before the entire gauge has turned martensitic.

3.4. Origin of the large variation in global mechanical behavior

The difference between the nature of the deformation of the two types of orientations is captured entirely in the difference the martensite transformation takes through the two microstructures. The path of the transformation in both types of orientations is influenced by the local grain orientation and the redistribution of the local elastic stress field in adjacent grains once a grain transforms. For the 0° specimens, martensite transformations nucleate at multiple nearby sites, which often coalesce into a single front, propagating across the width of the sample gauge in a macroscopic Lüders-like band. When the almost contiguous transformation band in the 0° specimens encounters a transverse band of ⟨100⟩ grains, transformation halts, and the subsequent elongation increases the elastic strain (and hence the elastic stress) mostly in these ⟨100⟩ grains. Often, new martensite tends to nucleate on the opposite side of the ⟨100⟩ band, leaving behind trapped ⟨100⟩ islands in the wake of the transformation. (The increase in the stress as a band of ⟨100⟩ grains is encountered results in the rising edge, and stress relation once new martensite is formed on the other side of the ⟨100⟩ band results in the falling edge of an undulation in the stress plateau.) In contrast, as soon as the first grains transform, the entire gauge length of the 45° specimen becomes decorated with higher-strain criss-cross patterns (Fig. 6) that are 45° to the gauge direction. These patterns appear to be predictive of the progressive transformation and are predominantly composed of ⟨100⟩ grains (Fig. 5). Martensite nucleates in between one of these 45° criss-cross bands and propagates until it reaches another highly strained cross band. When this occurs, transformation halts until the stress increases to nucleate martensite in another valley in between a set of cross-hatched highly strained bands. Eventually a 45° criss-cross pattern of transformation emerges, the boundaries decorated by highly strained ⟨100⟩ grains. The first few grains in 45° and 0° specimens appear to transform at nearly the same applied stress (∼350 MPa), but the torturous, start–stop pathway of martensite transformation in the 45° specimen leads to the significantly greater stress for the onset of the macroscopic stress plateau as well as making it steeper, and shorter.

4. Conclusions

The insights gained here on the role of local grain orientation on the nature of the martensitic phase transformation in Nitinol give a much fuller understanding of the factors that influence superelastic response in Nitinol. Our study indicates microstructural level processes by which stresses can redistribute upon phase transformation, leading to stress "hot spots" in conventionally unexpected locations. Uneven stress distribution, and especially the stress hot spots, may strongly impact fatigue life and trigger unforeseen fractures. Specifically, the location and the orientation of difficult-to-transform ⟨100⟩ grains appear to play an enormous role in determining the mechanical response, especially in the superelastic regime, by resisting transformation and bearing progressively higher elastic stresses. Interaction of these grains with the martensite transformation front stalls it or redirects it and consequently alters mechanical response from theoretical predictions. When the concentration of the ⟨100⟩ type grains is low, as it is for the 0° and 90° specimens in this investigation, the stress plateaus are relatively flat and by end of the plateau most of the gauge is martensitic. The mechanical properties of these types of specimens do not deviate significantly from the predictions of single-crystal theories (Bhattacharya, 2003). But as the concentration of ⟨100⟩ grains rises the local stresses begin to diverge from the global stresses and the global mechanical response is progressively more sensitive to the local microstructure and begins to deviate from theoretical predictions.

Thermomechanical processing, through transformation and grain re-orientation, significantly alters the orientation of many grains, but because of elastic softness and inability to transform to martensite, we believe that these processes do not have a large impact on orientation and concentration of ⟨100⟩ grains. Hence, the concentration and orientation of these very influential grains is uncontrolled from strut-to-strut in Nitinol medical devices. Mechanical behavior of individual struts *in vivo* is critically affected by the particulars of the local and discontinuous microstructure. Unfortunately, it is not likely that all of these local microstructural effects can be fully incorporated in continuum mechanics based computational models of complex medical devices. This microstructural driven variability explains some of the reported deviation of mechanical response of NiTi components at high deformation from the prediction of FEA (Mehta et al., 2007).

Nevertheless, some the mechanical response variability, though still arising from local microstructural effects, can be related to average global texture. It is imperative that these differences in mechanical properties due to geometric orientation differences, as posed in the realistic example of open and closed configurations in Fig. 1, must be incorporated the continuum-based stent design models.

For example, the "open" and "closed" configuration stents shown in Fig. 1, fabricated from tubes that have undergone traditional tube drawing thermomechanical processes, have average crystallographic texture along the struts that are markedly different from each other and cannot be modeled with a common global stress–strain relationship. The struts

of stents in the "closed" configuration are along the drawing direction, and hence, as a first approximation, they will respond in accordance with the parameters listed in Table 1 for the 0° specimen; whereas the struts in the "open" configuration are cut along a steeply oblique direction to the tube axis, and hence the parameters listed for the 45° specimen will most likely result in more fidel predictions.

In summary, the observations of microstructural level effects on the global mechanical response investigated here is the beginning of a deeper understanding of the performance and the origin of some of the unpredicted failures of real world, superelastic Nitinol devices. We believe that effects of some of these microstructural driven deviations can be incorporated in continuum-based design models for more reliable NiTi endovascular stents and medical devices. However other mechanical response variability and unpredictability, including some of the unexpected fractures, originate in specific local microstructural morphology, cannot be eliminated easily.

REFERENCES

ASTM 2006. F 2082 — 06 standard test method for determination of transformation temperature of nickel–titanium shape memory alloys by bend and free recovery. In: ASTM International.

Bhattacharya, K., 2003. Microstructure of Martensite. Oxford University Press, Oxford.

Brinson, L.C., Schmidt, I., Lammering, R., 2004. Stress-induced transformation behavior of a polycrystalline NiTi shape memory alloy: micro and macromechanical investigations via in situ optical microscopy. J. Mech. Phys. Solids. 52, 1549–1571.

Cheng, C.P., Choi, G., et al., 2010. The effect of aging on deformations of the superficial femoral artery resulting from hip and knee flexion: potential clinical implications. J. Vasc. Interv. Radiol. 21, 195–202.

Cheng, C.P., Wilson, N.M., et al., 2006. In vivo mr angiographic quantification of axial and twisting deformations of the superficial femoral artery resulting from maximum hip and knee flexion. J. Vasc. Interv. Radiol. 17, 979–987.

Duerig, T.W., Pelton, A.R., et al., 1996. The utility of superelasticity in medicine. Bio-Med. Mater. Eng. 6, 255–266.

Eucken, S., Duerig, T.W., 1989. The effects of pseudoelastic prestraining on the tensile behaviour and two-way shape memory effect in aged NiTi. Acta Metall. 37, 2245–2252.

Hasan, M., Schmahl, W.W., et al., 2008. Hard X-ray studies of stress-induced phase transformations of superelastic NiTi shape memory alloys under uniaxial load. Mater. Sci. Eng. A. 481–482, 414–419.

http://nitinoluniversity.com/open-stent-design/.

Jung, Y., Papadopoulos, P., et al., 2004. Constitutive modelling and numerical simulation of multivariant phase transformation in superelastic shape-memory alloys. Int. J. Numer. Meth. Eng. 60, 429–460.

Kröger, A., Wernhardt, R., et al., 2006. In situ transmission electron microscopy-investigations on the strain-induced B19'-phase in NiTi shape memory alloys structured by focused ion beam. Mater. Sci. Eng. A. 438–440, 513–516.

Liu, Y., Xie, Z.L., et al., 1999. Effect of texture orientation on the martensite deformation of NiTi shape memory alloy sheet. Acta Mater. 47, 645–660.

McNaney, J.M., Imbeni, V., et al., 2003. An experimental study of the superelastic effect in a shape-memory Nitinol alloy under biaxial loading. Mech. Mater. 35, 969–986.

Mehta, A., Gong, X.-Y., et al., 2007. Understanding the deformation and fracture of nitinol endovascular stents using in situ synchrotron X-ray micro-diffraction. Adv. Mater. 19, 1183–1186.

Miyazaki, S., Kimura, S., et al., 1984. The habit plane and transformation strains associated with the martensitic transformation in Ti–Ni single crystals. Scripta Metall. 18, 883–888.

Mulder, I.J.H., Thoma, P.E., et al., 1994. Anisotropy of thermal fatigue properties of cold-rolled TiNi sheet. Materials Characterization 32, 161–168.

Ono, N., Sato, A., 1988. Plastic deformation governed by the stress induced martensitic transformation in polycrystals. Trans. Jpn. Inst. Metals. 29, 267–273.

Ono, N., Satoh, A., et al., 1989. A discussion on the mechanical properties of shape memory alloys based on a polycrystal model. Trans. Jpn. Inst. Metals. 30, 756–764.

Pelton, A.R., Barney, M., Bronfenbrenner, D., Barney, M., Mehta, A., unpublished results.

Pelton, A.R., DiCello, J., et al., 2000. Optimisation of processing and properties of medical-grade Nitinol wire. Min. Invas. Ther. & Allied Technol. 9, 107–118.

Pelton, A.R., Schroeder, V., et al., 2008. Fatigue and durability of nitinol stents. J. Mech. Behav. Biomed. Mater. 1, 153–164.

Rebelo, N., Perry, M., 2000. Finite element analysis for the design of nitinol medical devices. Min. Invas. Ther. & Allied Technol. 9, 453–462.

Robertson, S.W., Gong, X.Y., et al., 2006. Effect of product form and heat treatment on the crystallographic texture of austenitic Nitinol. J. Mater. Sci. 41, 621–630.

Robertson, S.W., Mehta, A., et al., 2007. Evolution of crack-tip transformation zones in superelastic Nitinol subjected to in situ fatigue: a fracture mechanics and synchrotron X-ray microdiffraction analysis. Acta Mater. 55, 6198–6207.

Schillinger, M., Sabeti, S., et al., 2006. Balloon angioplasty versus implantation of Nitinol stents in the superficial femoral artery. New Engl. J. Med. 354, 1879–1888.

Shaw, J.A., Kyriakides, S., 1997. On the nucleation and propagation of phase transformation fronts in a NiTi alloy. Acta Mater. 45, 683–700.

Tamura, N., Celestre, R.S., et al., 2002. Submicron X-ray diffraction and its applications to problems in materials and environmental science. Rev. Sci. Instr. 73, 1369–1372.

Wick, A., Vöhringer, O., et al., 1995. The bending behavior of NiTi. J. de Phys. 5, 789–794. IV Coll. C8.

Young, M.L., Wagner, M.F.X., et al., 2010. Phase volume fractions and strain measurements in an ultrafine-grained NiTi shape-memory alloy during tensile loading. Acta Mater. 58, 2344–2354.